This article has been accepted for publication in a future issue of this journal, but has not been fully edited. Content may change prior to final publication. Citation information: DOI 10.1109/TPWRS.2018.2876466, IEEE Transactions on Power Systems

An Accurate Charging Model of Battery Energy Storage

Hrvoje Pandžić, *Senior Member, IEEE* and Vedran Bobanac

***Abstract*—Battery energy storage is becoming an important part of modern power systems. As such, its operation model needs to be integrated in the state-of-the-art market clearing, system operation and investment models. However, models that commonly represent operation of a large-scale battery energy storage are inaccurate. A major issue is that they ignore the dependency of the charging power on the battery state of energy. Consequently, market players might suffer great monetary losses for not being able to follow their day-ahead schedule and/or deliver the scheduled reserves.**

In order to bridge the gap between very detailed low-level battery charging constraints and high-level battery operation models used in the literature, this paper examines a dependency of battery charging ability on its state of energy. It proposes a laboratory procedure, which can be used for any battery type and technology, to obtain this dependency. It also formulates an accurate linear battery charging model, which closely approximates the real-life battery charging constraints. The proposed battery charging model is compared against the models commonly used in the literature. Battery operation schedules obtained by all the models are compared against experimentally obtained results in order to assess the value of the proposed model in real life.

***Index Terms*—Battery energy storage, battery charging, electricity market, laboratory verification.**

I. Introduction

Massive integration of renewable energy sources has severe implications on power system scheduling and operation. Namely, reduced online dispatchable generation capacity might not be able to deal with inherent variability and uncertainty of the output of renewable generation. Energy storage is a new resource that can perform load-following tasks and provide flexibility to the power system. Although energy storage technology has been a part of the power system for many decades in form of pumped hydro power plants, battery energy storage has become attractive due to declining prices, fast response and modularity of batteries. Department of Energy's Global Energy Storage Database as of November 2017 reports 725 operational battery energy storage projects worldwide with overall capacity of 1,500 MW [1]. This is in line with Navigant's report from 2014, which forecasts a rapid increase of installed battery storage capacity to 14,000 MW in 2022 [2].

The authors are with the Faculty of Electrical Engineering and Computing University of Zagreb, Croatia. This work was carried out within projects Electric Vehicle BAttery Swapping Station - EVBASS, funded by the Croatian Science Foundation under grant IP-2014-09-3517, and Smart Integration of RENewables - SIREN, funded by the Croatian Science Foundation and the Croatian TSO (HOPS) under grant I-2583-2015.

A. Literature Review

Since utility-scale battery storage has only been around for couple of years at best, there is a lack of publicly available data on battery storage operation. This results in fairly simple battery models being used within the power system economics community. A transmission-constrained unit commitment model expanded with battery energy storage is presented in [3]. This model simulates day-to-day operation of a vertically integrated power system in order to make near-optimal investment decision in energy storage. In [4], the authors use large-scale batteries to implement post-contingency corrective control actions. Distributed batteries are used to preserve system stability after a contingency and to provide required time for redispatch of generators. This work is expanded with intertemporal constraints in [5], where batteries provide corrective control in a unit commitment formulation.

Battery energy storage is often paired with wind farms to provide stable output and improve market bidding outcomes. A coordinated wind farm-battery operational dispatch that considers wind uncertainty is proposed in [6]. Statistical analysis of the distribution of wind output forecast errors is used to determine optimal battery power capacity, while the optimal energy capacity is chosen ex ante, based on the net present values of investments. On the other hand, [7] presents a control methodology for a wind farm and a battery storage to provide primary and secondary frequency control. A feedback control of the battery state of charge is used to reduce the size and extend the lifetime of the battery storage.

Batteries are also used in microgrid investment and operation models. A model that finds the optimal mix of renewable generation and battery capacity for an isolated microgrid is presented in [8]. Robust optimization approach is used to accommodate uncertainty related to demand and output of renewable generation. The case study examines both li-ion and lead-acid battery technologies. Optimal microgrid bidding strategy in the day-ahead market is proposed in [9]. Uncertainty related to market prices and outputs of intermittent renewable generation is tackled using a hybrid stochastic/robust optimization.

Battery charging/discharging models are also essential for scheduling the demand of electric vehicles. Many papers, such as [10] and [11], formulate optimal electric vehicle aggregator bidding models in electricity markets. In these papers, aggregator's objective is to minimize charging cost for its fleet. Since it is assumed that the aggregator can influence market prices, optimal bids are determined in the upper-level problem, while the market clearing is simulated in the lower-

This article has been accepted for publication in a future issue of this journal, but has not been fully edited. Content may change prior to final publication. Citation information: DOI 10.1109/TPWRS.2018.2876466, IEEE Transactions on Power Systems

level problem. On the other hand, in [12] an aggregator of electric vehicles is considered to be a price taker, i.e. it cannot influence market prices. It performs arbitrage between the day-ahead and real-time markets. All three electric vehicle aggregator models, [10]– [12], consider uncertainties related to renewable generation and behavior of electric vehicle drivers.

Another line of research focused on electric vehicle batteries are electric vehicle battery swapping stations. Optimal operation and services scheduling of an electric vehicle battery swapping station is modeled in [13]. This model examines scheduling of the battery swapping station services considering the prices in electricity markets, as well as the expected battery swap demand. A method for locating and sizing battery swapping stations in distribution networks is presented in [14]. This method maximizes net present value of a battery swapping station investment project considering the life cycle cost criterion.

B. On Battery Charging Models

All the papers in the literature review above consider battery energy storage modeling at the high level, meaning that they integrate a simple representation of physicochemical battery constraints into large operational or investment models. On the other hand, there are many detailed battery models, which aim at describing the processes within batteries as accurately as possible. However, such models are not suitable for integration in the high-level optimization problems due to their complexity. A good overview of detailed battery models is given in [15], which classifies them as: electrochemical, electrical-circuit, stochastic and analytical models. For instance, a very detailed electrochemical model for li-ion batteries has been developed by Doyle et al. [16]. This model is implemented in a computer program called Dualfoil [17] and it requires over 50 battery-related input parameters (e.g. thickness of the electrodes), but is very accurate and therefore often used for benchmarking other battery models [15]. In this paper we use experimental results which are considered more reliable than any computer simulation.

A simple battery model developed for usage in energy simulations and embedded smart control systems is presented in [18]. Major drawback of this approach is that it considers only the constant-current phase of the battery charging characteristic and neglects the constant-voltage phase, which is normally present whenever a battery is being fully charged. The model proposed in [18] is compared to a kinetic battery model (KiBaM) in [19]. The KiBaM model is actually a first-order approximation of the diffusion model from [20], as shown in [15]. However, due to their complexity, neither of these models is suitable for usage in the high-level optimization problems.

An approach most similar to ours in presented in [21], where a MILP battery model with piecewise linear constraints is applied to energy arbitrage. However, there are some important differences. Authors of [21] start from a low-level battery model that takes into account thermodynamics, charge transfer, mass transport, etc. The model parameters are obtained from the manufacturer's specification sheets and the final model is validated only by comparison with the manufacturer's discharge voltage characteristic. On the other hand, we use experimental data obtained in our own laboratory, which provides an exhaustive insight into battery's behaviour and characteristics. We believe that our constraints are more fundamental and realistic, as the model in [21] uses the same constraints for both charging and discharging power limits, which we show are substantially different.

C. Contributions and Paper Organization

This paper formulates a linear program that captures variable battery charging limit and can be incorporated in any battery operation and/or investment planning model. It bridges the gap between the high-level studies, i.e. operation and investment models, that require simple battery operation models on one hand, and detailed laboratory models that correctly capture the physics of the battery on the other hand. A dedicated laboratory testbed is developed to accurately control battery charging and discharging process. The testbed contains an advanced tailor-made bidirectional AC-DC converter with precise current and voltage measurements. The converter enables performing rigorous charging and discharging patterns. In this research, we use it to obtain an accurate battery charging curve needed to derive correct input parameters for the battery model. The three battery models tested in this paper are: (i) the constant charging power limit, as commonly found in research studies; (ii) charging power limit with linear reduction at the constant voltage part of the charging curve, as proposed in [12]; (iii) piecewise linear approximation of the available charging energy, as proposed in this paper. To demonstrate the effectiveness, these three battery models are incorporated into an optimal energy storage market bidding model. The quality of the solutions is verified by applying the obtained charging/discharging schedules to a battery at the laboratory testbed in order to check their feasibility.

Contributions of the paper are:

1) Definition of a laboratory procedure for obtaining accurate dependency of the battery charging capacity on its state of energy.
2) Formulation of a piecewise linear approximation of the battery charging capacity suitable for high-level operational and investment models.
3) Analysis of the feasibility and cost-effectiveness of the obtained charging/discharging schedules within the optimal energy storage bidding model using the laboratory testbed.

The rest of the paper is organized as follows. Section II describes our laboratory testbed, while Section III provides an insight in some fundamental li-ion battery characteristics important for understanding the proposed battery charging model. Optimal battery energy storage bidding model using different battery charging constraints is formulated in Section IV. Case study with laboratory verification of the obtained battery charging/discharging schedules is presented in Section V. Finally, the conclusions and recommendations are provided in Section VI.

This article has been accepted for publication in a future issue of this journal, but has not been fully edited. Content may change prior to final publication. Citation information: DOI 10.1109/TPWRS.2018.2876466, IEEE Transactions on Power Systems

II. Laboratory Testbed

For the purpose of experimenting with various batteries, an advanced grid-tied bidirectional AC-DC converter has been constructed. This specially designed converter allows implementation of any battery charging/discharging pattern. The basic specifications of the converter are:

- Nominal output power: 1 kW
- Output voltage: 0 to 20 V DC
- Output current: -50 to 50 A DC
- Input: 50 Hz, 230 V AC

Input/output current/voltage are measured by analog signals (0-10 V DC) and digital signals (isolated USB or RS-485). Resolution of the voltage and current measurements is 0.6 mV and 5.8 mA. Accuracy is improved by the remote battery voltage sensing.

The converter is connected to the host PC using National Instruments (NI) equipment. Communication takes place over NI cRIO[1] via Ethernet, while the converter is supervised and controlled over a SCADA[2] system implemented in NI LabVIEW[3].

The converter has a three-stage topology which consists of: (i) a bidirectional grid inverter; (ii) a resonant high-frequency (HF) transformer; and (iii) an output bidirectional interleaved buck-boost converter. This topology is shown in Fig. 1.

Physical realization of the converter is shown in Fig. 2, where each part is marked with a different color. Note that the buck-boost part is for the most part not visible, as it is located under the control board. Connection between the control board and the NI cRIO is clearly visible. Cable that connects the converter to the grid can be seen in the lower left part of the figure (marked orange), while the 18650 li-ion battery cell under test is also located on the left-hand side.

We consider li-ion as the most popular battery technology today due to its declining prices and favorable characteristics (e.g. high energy density, fast charging possibility etc.) [22]. The described converter and the 18650 li-ion cell have been used to obtain all the experimental results presented in this paper. Since the experiment is focused on the battery characteristics, all the voltage and current measurements are taken at the battery side of the converter, i.e. at the li-ion cell under test.

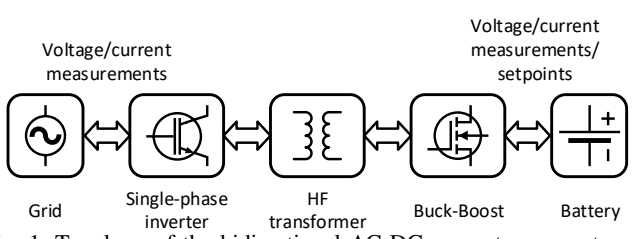

Fig. 1. Topology of the bidirectional AC-DC converter converter

[1]cRIO (compact Reconfigurable Input Output) is a real-time industrial controller

[2]SCADA (Supervisory Control And Data Acquisition)

[3]LabVIEW (Laboratory Virtual Instrument Engineering Workbench)

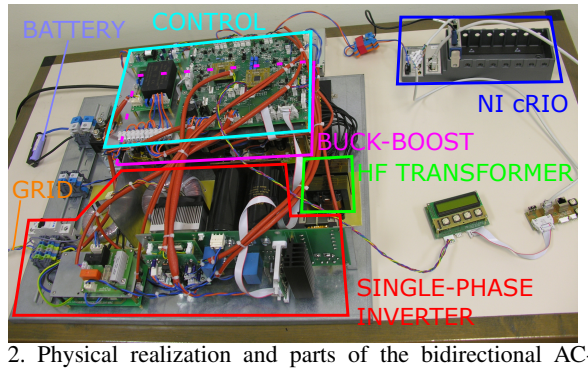

Fig. 2. Physical realization and parts of the bidirectional AC-DC converter

III. Li-ion Battery Characteristics

Li-ion batteries are normally charged with the constant-current-constant-voltage (CC-CV) characteristic [23], [24]. This characteristic consists of two phases. In the first phase, the charging current is constant, while the voltage gradually rises to a certain predefined threshold (charging voltage). In the second phase, the voltage is kept constant at the threshold value while the current gradually decreases. Full charge is reached after the current drops to cca. 3% of the battery's Ampere-hour (Ah) rating [24]. Experimentally obtained battery charging characteristics can be seen in Fig. 3 for the charging currents of 1C and 0.2C. C-rate is determined by the battery capacity in Ah. For the battery cell at hand, the measured capacity amounts to 2.8 Ah, so the current of 1C corresponds to 2.8 A, while 0.2C corresponds to 0.56 A.

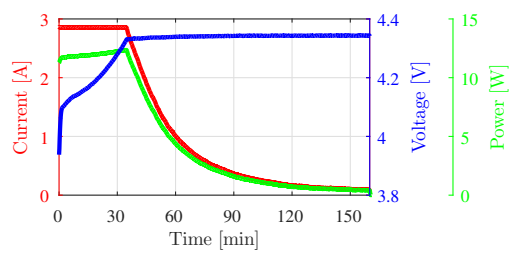

(a) Charging current 2.8 A (1C)

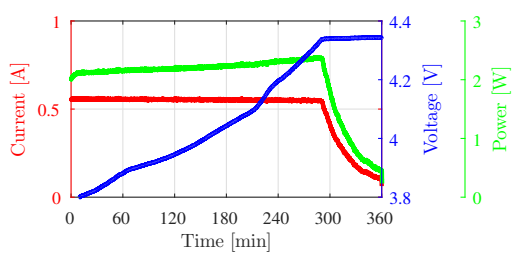

(b) Charging current 0.56 A (0.2C)

Fig. 3. Battery charging characteristic

Battery state of charge is a measure of the amount of charge stored in a battery with respect to the charge that the battery contains when fully charged. State of charge gives the user an indication of how much longer a battery will last before it needs recharging [25]. In consumer electronics and some electric vehicles state of charge is displayed in percentages. In real-time implementations, battery state of charge is not straightforward to determine and there is a number of papers

This article has been accepted for publication in a future issue of this journal, but has not been fully edited. Content may change prior to final publication. Citation information: DOI 10.1109/TPWRS.2018.2876466, IEEE Transactions on Power Systems

that tackle this problem with an aim to increase accuracy of the state of charge estimation. A review of different approaches and methods for state of charge estimation can be found in [26], [27]. The most common method for state of charge estimation is coulomb counting, which is based on integration of the charging/discharging current, see e.g. [28]. Coulomb counting method can be described by the following relation:

$$\begin{aligned} soc_t^{\%} =& soc_{t-1}^{\%} + \eta^{\mathrm{I}} \cdot \frac{100}{C^{\mathrm{I}}} \int_{t-1}^{t} ch^{\mathrm{I}}(\tau) d\tau \\ &- \frac{100}{C^{\mathrm{I}}} \int_{t-1}^{t} dis^{\mathrm{I}}(\tau) d\tau, \end{aligned} \tag{1}$$

where $soc_t^{\%}$ is state of charge (expressed in percentages), t index of time periods, η^{I} coulombic efficiency, C^{I} the battery charge capacity (Ah), ch^{I} (A) and dis^{I} (A) charging and discharging currents (both always assumed positive). Equation (1) counts Ampere-hours (Ah) that enter and exit the battery[4]. In literature, one may often find the term state of charge being used for counting Watt-hours (Wh). While similar, counting Ah and Wh is not the same, so to avoid this discrepancy we adopt the term *state of energy*, which is used in [12], [29]. Furthermore, using state of energy instead of state of charge is justified by the fact that participants in energy markets trade energy (Wh) and not electric charge (Ah). State of energy is determined by the relation analogous to (1), as follows:

$$\begin{aligned} soe_t^{\%} =& soe_{t-1}^{\%} + \eta^{\mathrm{E}} \cdot \frac{100}{C^{\mathrm{E}}} \int_{t-1}^{t} ch(\tau) d\tau \\ &- \frac{100}{C^{\mathrm{E}}} \int_{t-1}^{t} dis(\tau) d\tau, \end{aligned} \tag{2}$$

where $soe_t^{\%}$ is state of energy (expressed in percentages), η^{E} energy efficiency, C^{E} the battery energy capacity (Wh), ch (W) and dis (W) charging and discharging powers (both always assumed positive).

If a battery is a part of the power system, it interacts with it in terms of power and energy. Therefore, eq. (2) is transformed to accommodate state of energy (soe_t) in Wh:

$$soe_t = soe_{t-1} + \eta^{\mathrm{E}} \int_{t-1}^{t} ch(\tau) d\tau - \int_{t-1}^{t} dis(\tau) d\tau. \tag{3}$$

Battery efficiency can be divided into: (i) coulombic, (ii) voltaic, and (iii) energy efficiency. Coulombic efficiency η^{I}, used in (1), is the ratio of the total charge extracted from the battery (Ah) to the total charge injected in the battery (Ah) over a full charge/discharge cycle [24]. Voltaic efficiency, η^{V}, is the ratio of the average discharging voltage and the average charging voltage [24]. Charging voltage is always higher than the discharging voltage due to the battery's internal resistance. Fig. 4 displays experimentally obtained battery charging and discharging voltage curves forming a kind of hysteresis. Higher charging currents shift charging voltage further upwards and higher discharging currents shift discharging voltage further downwards. This indicates that voltage efficiency reduces with higher (dis)charging currents. Finally, energy efficiency η^{E}, used in (2) and (3), can be defined as the ratio of the total energy extracted from the battery (Wh) and the total energy injected in the battery (Wh) over a full charge/discharge cycle. Energy efficiency is the lowest of the three efficiencies as it encompasses both coulombic and voltaic efficiency.

[4]One coulomb equals one Ampere-second, thus the terms coulomb counting and coulombic efficiency.

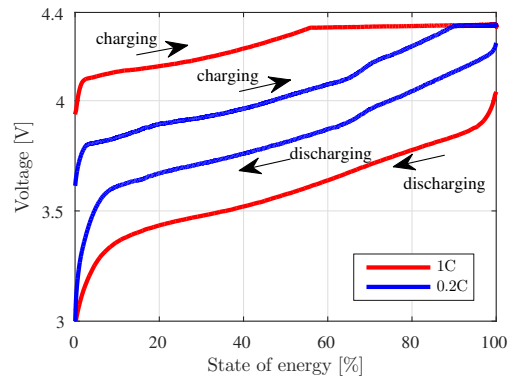

Fig. 4. Battery voltage hysteresis

Efficiencies are very dependent on the value (or profile) of the charging/discharging currents. This is especially the case for voltaic and, consequently, energy efficiency, as can be concluded from the above discussion and Fig. 4. Physical explanation for the efficiency variability are losses that are always present to a certain extent as a consequence of the battery's internal resistance. Naturally, higher currents cause higher losses. Therefore, energy stored in the battery is always lower than the energy input during a (full) charge cycle. Likewise, energy extracted from the battery during a (full) discharge cycle is always lower than the energy that was stored in the battery. In order to account for this, the overall (round-trip) energy efficiency of the battery is often decomposed into the charging and the discharging efficiency. This allows one to take into account the influence of charging current on charging efficiency (and discharging current on discharging efficiency) by calculating power losses over the battery's internal resistance (see e.g. [30]).

In this paper we use single overall energy efficiency η^{E}, which is accurately determined from the experimental data as follows. A full charging/discharging cycle is applied to the battery while measuring electrical power charged ch (W) and discharged dis (W). Round-trip energy efficiency is then obtained as:

$$\eta^{\mathrm{E}} = \frac{\int_0^{T_{fd}} dis(\tau) d\tau}{\int_0^{T_{fc}} ch(\tau) d\tau}, \tag{4}$$

where T_{fd} and T_{fc} are times to fully discharge and charge the battery, respectively. State of energy calculated by (3) is then always the useful energy that can be withdrawn from the battery. Knowing η^{E} is important as it determines the amount of energy that has to be purchased in the market during the low-price time periods in order to be able to deliver the desired amount of energy during the high-price time periods. In the considered case, η^{E} for the desired combinations of charging/discharging currents should be determined from the most recent measured data.

This article has been accepted for publication in a future issue of this journal, but has not been fully edited. Content may change prior to final publication. Citation information: DOI 10.1109/TPWRS.2018.2876466, IEEE Transactions on Power Systems

IV. Battery Operation Formulations

In order to compare battery charging models from the literature with the proposed one, we formulate a rather simple battery energy storage bidding model. Only the day-ahead energy market is considered, where battery energy storage maximizes its profit by performing energy arbitrage. The battery storage is a price taker and cannot affect market prices, which are known in advance, i.e. no price uncertainty is considered. The following three subsections formulate three battery storage models which differ by the way they incorporate battery charging constraints: (i) constant charging power limit, which is the most commonly used in literature, (ii) charging power limit with linear reduction, as proposed in [12], and (iii) variable charging energy limit, which is the one proposed in this paper.

A. Model with Constant Charging Power Limit (Baseline Model)

Objective function of the optimal battery energy storage bidding problem is to maximize profit by exercising arbitrage:

$$\text{maximize} \sum_{t \in T} \lambda_t \cdot (dis_t - ch_t) \cdot \Delta t \tag{5}$$

where λ_t are hourly market prices, dis_t is power sold in the market, and ch_t power purchased in the market. Objective function (5) is constrained by:

$$ch_t \leq P^{\text{ch}}, \quad \forall t \in T \tag{6}$$

$$dis_t \leq P^{\text{dis}}, \quad \forall t \in T \tag{7}$$

$$soe_t = soe_{t-1} + \Delta t \cdot ch_t \cdot \eta^{\text{E}} - \Delta t \cdot dis_t, \quad \forall t \in T \backslash 1 \tag{8}$$

$$soe_1 = soe_0 + \Delta t \cdot ch_1 \cdot \eta^{\text{E}} - \Delta t \cdot dis_1, \tag{9}$$

$$soe_t \leq C^{\text{E}}, \quad \forall t \in T \tag{10}$$

$$soe_T \geq soe_0, \tag{11}$$

$$ch_t, dis_t, soe_t \geq 0, \quad \forall t \in T. \tag{12}$$

Constraints (6) and (7) represent battery charging and discharging constraints, where P^{ch} and P^{dis} are parameters representing maximum battery charging and discharging powers. Equation (8) calculates the battery state of energy, soe_t, based on the state of energy in the previous time period and (dis)charged energy, while considering battery energy efficiency η^{E}. Δt is a length of the time period, e.g. 1 h, used to obtain energy quantity from the power variables ch_t and dis_t. Equation (9) calculates the state of energy at the first time period based on the initial state of energy soe_0. Equations (8) and (9) correspond to (3), with the difference that integrals are calculated by the rectangle method which renders (8)-(9) algebraic. Constraint (10) limits the state of energy using parameter C^{E} (battery energy capacity in Wh), while (11) ensures that the final state of energy is not lower than the initial one. Finally, (12) imposes non-negativity on the variables.

Model (5)-(12) is the most commonly used (and simplest) battery storage model in the power system economics literature, used in [3]– [11], [13], [14], and many others. From now on, this model is referred to as the **baseline model** that needs to be outperformed. The opportunity for enhancement lies in a more rigorous modeling of the charging limit, which reduces for state of energy levels above a certain value. This is a direct result of the battery charging characteristic, which consists of two distinctive parts, constant-current and constant-voltage, as shown in Fig. 3. As battery charges with constant current, its voltage increases. Once the battery reaches its voltage limit, the current starts decreasing to keep the battery voltage at the limit (4.35 V in Fig. 3). Consequently, the charging power, obtained by multiplying the current and the voltage, reduces drastically as the energy stored in the battery approaches its maximum value.

B. Model with Reducing Charging Power (Linear CC-CV Model)

A more accurate representation of the battery charging power constraint (6) is proposed in [12], where the authors acknowledge the reduced charging capacity after switching to the constant-voltage mode when charging a battery.

The linear form of the charging power dependency on the battery state of energy is formulated as in [12]:

$$ch_t \leq P^{\text{ch}}, \quad \forall t \in T, \tag{13}$$

$$ch_t \leq P^{\text{ch}} \cdot \frac{C^{\text{E}} - soe_t}{C^{\text{E}} - SOE^{\text{cc,cv}}}, \quad \forall t \in T, \tag{14}$$

where $SOE^{\text{cc,cv}}$ is a parameter denoting the state of energy at which the constant-current switches to the constant-voltage charging scheme. Constraint (13) sets maximum charging rate for all states of energy, while constraint (14) imposes a stricter charging limit for states of energy above $SOE^{\text{cc,cv}}$. The stricter charging limit linearly decreases from P^{ch} at $soe_t = SOE^{\text{cc,cv}}$ to zero at $soe_t = C^{\text{E}}$.

From now on, this model is referred to as the **linear CC-CV model**. The formulation of the bidding problem using the linear CC-CV model is:

$$\text{Maximize} \quad (5)$$

subject to

$$(7) - (12), (13), (14)$$

C. Model with Energy Charging Limit (Energy Charging Model)

A new representation of the battery charging capacity constraint proposed in this paper is based on curves in Fig. 5, which display battery's ability to absorb energy as a function of the current state of energy. Δsoe indicates how much energy can be charged into the battery in the following time step. One hour is chosen as a standard time step used in most electricity markets, but other time steps can be used analogously. Δsoe characteristic in Fig. 5 is derived from the CC-CV characteristic in Fig. 3. For lower charging currents (e.g. 0.2C), during the constant-current phase, the Δsoe characteristic slowly rises. As the current decreases, the ability of the battery to absorb energy reduces. For higher charging currents (e.g. 1C) there is no rising part of the Δsoe curve, since the constant-current phase is shorter than one hour.

Nonlinear soe–Δsoe curves from Fig. 5 can be approximated by piecewise linear functions. An example is shown in

This article has been accepted for publication in a future issue of this journal, but has not been fully edited. Content may change prior to final publication. Citation information: DOI 10.1109/TPWRS.2018.2876466, IEEE Transactions on Power Systems

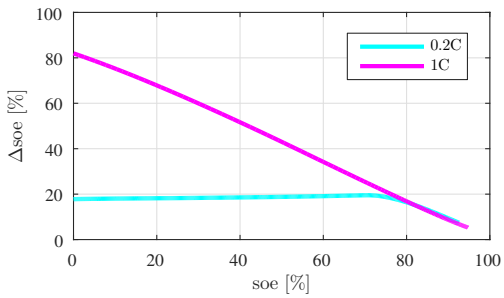

Fig. 5. Battery hour-ahead energy charging ability

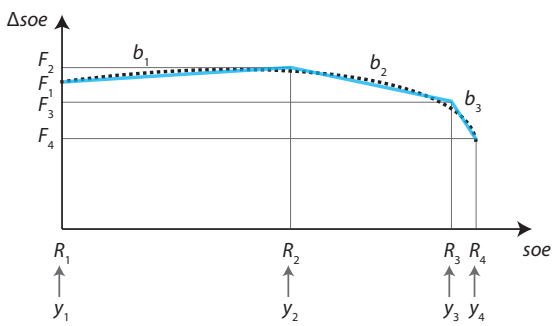

Fig. 6. Piecewise linear approximation of a soe–Δsoe function.

Fig. 6, where the dashed black line represents a nonlinear function being approximated by the solid blue segments. Pieces of the blue curve in Fig. 6 have monotonically decreasing slope coefficients as the state of energy increases. This is an important property since higher energy charging ability increases the value of the objective function (5). Therefore, this piecewise linear approximation can be modeled without using binary variables as follows:

$$soe_t = \sum_{i=1}^{I-1} soe_{t,i}, \quad \forall t \in T \tag{15}$$

$$soe_{t,i} \leq R_{i+1} - R_i, \quad \forall t \in T, i \in I \tag{16}$$

$$\Delta soe_t = F_1 + \sum_{i=1}^{I-1} \frac{F_{i+1} - F_i}{R_{i+1} - R_i} \cdot soe_{t-1,i}, \quad \forall t \in T \tag{17}$$

$$ch_t \leq \frac{\Delta soe_t}{\Delta t \cdot \eta^{\mathrm{E}}}, \quad \forall t \in T \tag{18}$$

Equation (15) decomposes battery state of energy into $I-1$ segments, where I is the number of breakpoints of the piecewise function in Fig. 6. Energy limit of each state of energy segment, $soe_{t,i}$, is enforced in constraint (16). Equation (17) determines maximum energy charging ability of the battery at each time period, while (18) represents corresponding power constraint. If the battery is empty, its energy charging ability is equal to F_1. If a portion of any $soe_{t-1,i}$ is greater than zero, it will affect the battery energy charging ability. Since reduced energy charging ability has a negative impact on the objective function value, auxiliary variables $soe_{t,i}$ will start *filling* from the lowest i index. For example, in Fig. 6, when charging an empty battery, segment b_1 will be used first, as it increases the energy charging ability of the battery. Next, segment b_2 will be used as it reduces the battery charging ability less than segment b_3.

From now on, this model is referred to as the **energy charging model**, as it considers the energy charging ability instead of the power limit. Formulation of the bidding problem using the energy charging model of the battery is:

$$\text{Maximize} \quad (5)$$

subject to

$$(7) - (12), (15) - (18)$$

In some applications it may happen that the higher battery charging ability reduces the objective function value. An example might be a strategic demand response bilevel model where battery storage is modeled as a follower in the lower-level problem. Also, it is possible that all the piecewise slopes of the approximated soe–Δsoe function are not monotonically decreasing as the state of energy increases (this can happen if a curve is approximated by many segments). In both cases, the soe–Δsoe curve needs to be approximated using binary variables. The proposed formulation based on Special Order Sets 2 (SOS2) is available in the Appendix.

In summary, we propose the following procedure for obtaining the energy charging model:

1) record battery charging/discharging characteristic for the desired charging/discharging currents;
2) obtain charging/discharging energies by integrating the charging/discharging power in time;
3) determine battery energy capacity and overall energy efficiency;
4) derive the $time$–soe curve from the charging energy characteristic;
5) derive soe–Δsoe curve from the $time$–soe curve;
6) approximate nonlinear soe–Δsoe curve by a piecewise-linear function in order to obtain parameters R_i and F_i required in (16) and (17).

V. Case Study

In this case study, optimal battery bidding models from Sections IV.A-C are applied to a fictional 10 MWh battery acting in the EPEX day-ahead market [31]. Day-ahead energy prices on January 15, 2018, which are used in simulations, are provided in Table I. The obtained (dis)charging schedules of the baseline model, the linear CC-CV model and the proposed energy charging model are verified for feasibility in a laboratory experiment. In this experiment, the assumed large-scale battery of 10 MWh energy capacity is represented with a single li-ion battery cell with 10 Wh energy capacity. Naturally, there are differences in voltage and current levels when using 10 Wh and 10 MWh battery. Percentage of losses in the larger battery may increase as a consequence of higher resistance due to interconnections between battery cells and packs. However, even if these differences are not negligible,

TABLE I. Prices in EPEX on January 15, 2018

Hour	Price (€/MWh)	Hour	Price (€/MWh)	Hour	Price (€/MWh)	Hour	Price (€/MWh)
1	29	7	41	13	50	19	54
2	31	8	54	14	49	20	52
3	28	9	53	15	38	21	46
4	23	10	48	16	37	22	37
5	25	11	50	17	37	23	41
6	27	12	50	18	43	24	36

This article has been accepted for publication in a future issue of this journal, but has not been fully edited. Content may change prior to final publication. Citation information: DOI 10.1109/TPWRS.2018.2876466, IEEE Transactions on Power Systems

the methodology introduced in our paper can still be used to assess battery of any size.

In order to be as realistic as possible, a new experiment is performed for every (dis)charging cycle, i.e. no experimental data is used more than once, even if the same (dis)charging pattern repeats. This accounts for uncertainties and measurement errors which are inherent to real battery operation.

In order to examine the effects of battery's energy-to-power ratio, i.e. its C-rate, we conduct the same simulations and laboratory experiments for 1C and 0.2C, resulting in theoretical battery (dis)charging times of 1 h and 5 h, respectively.

Overall battery energy efficiency η^{E} is determined experimentally by virtue of (4) and the following values were obtained:

- 1C case: $\eta^{\mathrm{E}} = 0.81$ (full cycle: 1C charge, 1C discharge),
- 0.2C case: $\eta^{\mathrm{E}} = 0.866$ (full cycle: 0.2C charge, 0.2C discharge).

As discussed in Section III, energy efficiency of the battery depends on the charging/discharging current, so including varying efficiency in the optimization problem would not be straightforward. Nevertheless, as shown in the sequel, battery energy storage is almost exclusively operated at maximum allowed currents of 1C and 0.2C. Therefore, we consider these fixed efficiencies to be credible parameters in our optimization models.

Experimental charging energy is obtained by integration of the measured charging power. This charging energy is then corrected for the overall energy efficiency (η^{E}) and scaled to 0-10 MWh span in order to simulate a 10 MWh battery. Values obtained in this fashion represent experimental charging energy and they are displayed by green bars in Figs. 7-8 (positive values are for charging and negative for discharging). Note that values of experimental charging energy for a certain hour can never exceed those determined by the simulation, i.e. the battery cannot charge more energy than scheduled to purchase. On the other hand, experimental charging energy lower than in simulations is a consequence of the battery's physicochemical constraints.

The battery is considered to be at 50% state of energy at the beginning of the optimization horizon and is required to end up at that level.

Parameter $SOE^{\mathrm{cc,cv}}$ used in the linear CC-CV model is determined from experimental charging characteristics and its values are:

- 1C case: $SOE^{\mathrm{cc,cv}} = 55.5\%$,
- 0.2C case: $SOE^{\mathrm{cc,cv}} = 89.7\%$.

As for the energy charging model, nonlinear soe–Δsoe curves from Fig. 5 are approximated by three and four piecewise linear curves, for 1C and 0.2C cases, respectively. Parameters R_i and F_i which define piecewise linear approximation are as follows:

- 1C case:
  $R_{1-4}(\%)$ =[0 23 94.7 100],
  $F_{1-4}(\%)$ =[82.3 65.8 4.6 0.0],
- 0.2C case:
  $R_{1-5}(\%)$ =[0 74 82 92.6 100],
  $F_{1-5}(\%)$ =[17.8 19.4 15.4 7.5 0.0].

Since these piecewise approximations have monotonically decreasing slopes, energy charging model proposed in IV-C is readily used. This model does not include binary variables and therefore it does not incur additional computational burden. Using IBM ILOG CPLEX 12.6.2. under GAMS 24.5.4. on an 8 GB RAM machine with INTEL i7-5500U CPU at 2.4 GHz, all the models are solved instantly.

A. 1C Maximum Charging Rate

This subsection presents the case study results for the maximum (dis)charging current of 1C. Fig. 7a displays results for the baseline model. Considering the charging power limit in (6), this model assumes that the battery can be fully charged within one hour. Experimental results, however, show that only about 8.2 MWh of electricity can in reality be charged within an hour. As a result, using the baseline model to schedule the battery energy storage in the day-ahead market leads to significant errors. In this case, energy that can be stored and delivered is 14.6% lower than assumed by the model (see Table II).

Fig. 7b displays battery charging schedule for the linear CC-CV model. This model better describes battery charging constraints and there are no deviations of the model output from the experimental data (state of energy graphs coincide). However, results from Table II suggest that the linear CC-CV model might be overly conservative, as the total energy stored and delivered (obtained by simulations) is lower than for the other two models (24.62 vs. 25.0 and 24.97). This conservatism can be overcome by introducing a parameter with a value greater than 1 to multiply the right-hand side of constraint (14). The best resulting profit of €257.67 is achieved if the value of this parameter is 1.4. However, the optimal value of this parameter can be determined only ex post and is not based on any actual battery parameter.

Results of the proposed energy charging model are displayed in Fig. 7c. The total simulated delivered energy amounts to 24.97 MWh. The deviation from 25.0 is caused by piecewise linear approximation of the soe–Δsoe curve. Comparison of the simulation and the experimental results show a 0.4% difference in the delivered energy, as seen in Table II (24.97 MWh vs. 24.87 MWh). This deviation is the result of the aforementioned uncertainties related to real battery operation, as separate experiments are used to obtain the model constraints and case study results. However, the overall delivered energy (experimentally obtained) is the highest among the three models.

An overview of the delivered electricity and the resulting profit for all three models is shown in Table II. The resulting profit is calculated as follows. The day-ahead profit, obtained in the simulations, is corrected for the balancing costs at each hour in the following way (based on the balancing rules set by the Croatian Energy Regulatory Agency [32]):

- If the day-ahead quantity is fully charged or discharged, there is no balancing costs.
- If the charging quantity cannot be met, the electricity not charged is sold at 70% of the purchasing price.
- If the discharging quantity cannot be met, the additional electricity is purchased at 140% of the day-ahead price.

This article has been accepted for publication in a future issue of this journal, but has not been fully edited. Content may change prior to final publication. Citation information: DOI 10.1109/TPWRS.2018.2876466, IEEE Transactions on Power Systems

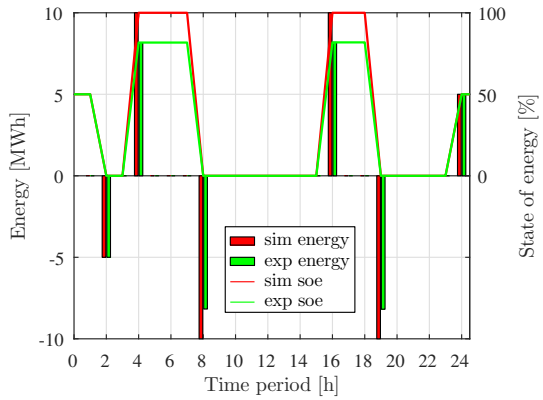

(a) Baseline model

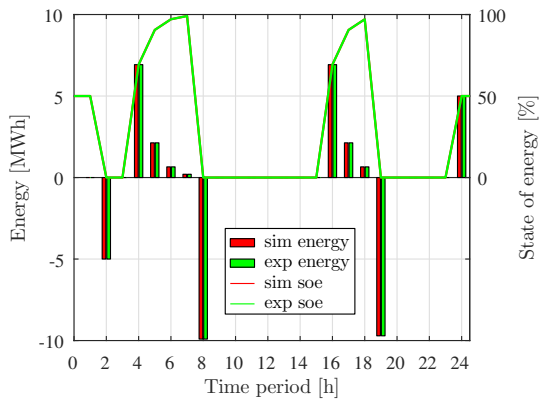

(b) Linear CC-CV model

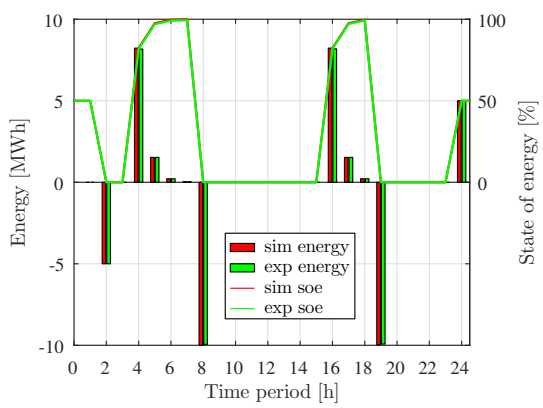

(c) Energy charging model

Fig. 7. Battery schedules for 1C rate

Since the baseline model cannot meet its charging schedule at hours 4, 8, 16 and 19, its €272.04 day-ahead profit is reduced to only €91.02. The linear CC-CV model is able to fully implement its day-ahead schedule and its simulation and experimental profits are the same. Due to real battery operation related uncertainties, the day-ahead profit of the energy charging model is reduced by €5.07, still resulting in the highest resulting profit of €259.64.

B. 0.2C Maximum Charging Rate

The battery simulation and experimental schedules for the three models are shown in Figs. 8a-8c. Both the baseline and the linear CC-CV models are unable to follow the charging schedule in hours 4 and 5. Consequently, the battery state of energy at the end of hour 6 is lower than needed and the discharging quantity at hour 13 cannot be met. Furthermore, insufficient charging ability in hours 22 and 24 result in the final state of energy of 41.2% (for both baseline and CC-CV models), which means that constraint (11) is not met in real operation. The main reason why the baseline and the linear CC-CV models underperform for 0.2C charging rate is the slowly rising power curve shown in Fig. 3b. Similarly as the baseline model, the linear CC-CV model does not take this into account and allows the highest charging power throughout the constant-current phase. However, in reality, when a battery is empty the charging power in the first hour is lower than the maximum charging power and increases with the state of energy until the beginning of the constant-voltage phase. This is clearly visible in hours 15-17 in Figs. 8a-8b, where the battery cannot be charged as much as anticipated in the simulations (note that the battery is empty at hour 14). This effect does not manifest at 1C charging rate of the linear CC-CV model because the constant-current phase is shorter than one hour. On the other hand, the proposed energy charging model is able to respect its day-ahead schedule at all time periods almost perfectly, resulting in the final state of energy of 49.9%. The biggest difference between the energy charging and the other two models occurs in hour 21, where the energy charging model sells less energy in order to be able to achieve 50% state of energy at the end of the day. The other two models overestimate battery charging capabilities, sell too much energy in hour 21 and cannot achieve the desired state of energy at the end of the day.

Since the battery starts the day at 50% state of energy and ends the day below this value, the total energy charged throughout the day is less than the total delivered energy, as seen in Table III (experimental values). In order to account for this error, it is assumed that the missing energy has to be purchased in the last hour in which the battery is idle, which is hour 23, at 140% of the day-ahead price. Other than this, the profits are calculated as described in Section V-A. The proposed energy charging model achieves the highest profit of €196.87, which deviates only 0.8% from the simulated

TABLE II. DELIVERED ENERGY AND RESULTING PROFIT COMPARISON FOR 1C RATE

Model		Baseline	Linear CC-CV	Energy Charging
Delivered energy (MWh)	Simulation	25.00	24.62	24.97
	Experiment	21.36	24.62	24.87
Charged energy (MWh)	Experiment	21.36	24.62	24.87
Resulting profit (€)	Simulation	272.04	249.51	264.71
	Experiment	91.02	249.51	259.64

TABLE III. DELIVERED ENERGY AND RESULTING PROFIT COMPARISON FOR 0.2C RATE

Model		Baseline	Linear CC-CV	Energy Charging
Delivered energy (MWh)	Simulation	15.00	14.89	14.10
	Experiment	14.90	14.79	14.07
Charged energy (MWh)	Experiment	14.01	13.91	14.06
Resulting profit (€)	Simulation	202.39	196.79	198.44
	Experiment	165.05	159.59	196.87

This article has been accepted for publication in a future issue of this journal, but has not been fully edited. Content may change prior to final publication. Citation information: DOI 10.1109/TPWRS.2018.2876466, IEEE Transactions on Power Systems

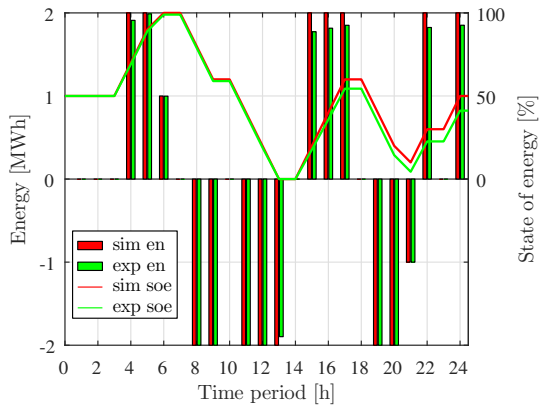

(a) Baseline model

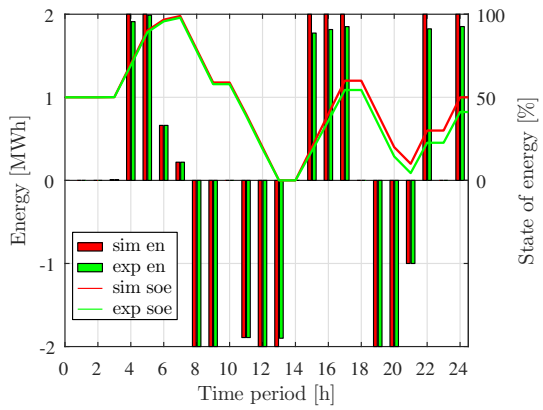

(b) Linear CC-CV model

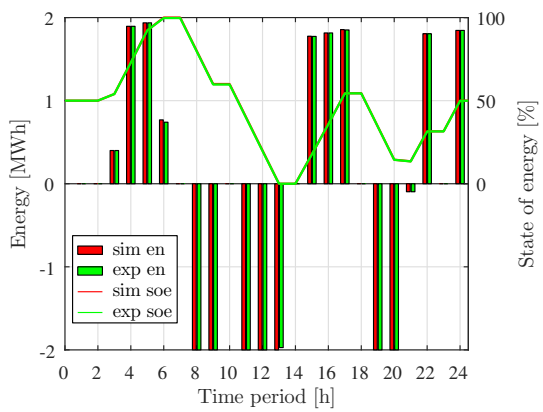

(c) Energy charging model

Fig. 8. Battery schedules for 0.2C rate

profit. On the other hand, the baseline and the linear CC-CV models have much lower profits (€165.05 and €159.59) and higher deviations from the simulation results (18.4% and 18.9%, respectively). This is the result of aggressive charging schedules that cannot be met in the experiment.

VI. Conclusion

This paper introduces a laboratory procedure to obtain accurate dependency of the battery charging capacity on its state of energy. This dependency is the basis for the proposed energy charging model introduced in Section IV-C.

For 1C rate, the baseline model is unable to deliver 14.6% of its (dis)charging quantities due to oversimplification of the charging constraint. On the other hand, the linear CC-CV model is able to fully fulfill its day-ahead schedule. However, this schedule is over-conservative and the profit of the battery owner is 3.9% lower than for the proposed energy charging model. The differences in the resulting profit are even higher for 0.2C, where the proposed model outperforms the other two by cca. 20%.

The main reason behind the accuracy of the proposed model is the inclusion of the soe–Δsoe curve in the model, which is essential for quantifying the energy a battery is able to absorb within a specific time period.

Future research will be focused on integration of the battery energy charging model into complex power system economics models, such as unit commitment and power system expansion models.

Appendix: Accurate Mixed-Integer Formulation

A general piecewise linear soe–Δsoe function is formulated using Special Order Sets 2 (SOS2) in the following way:

$$soe_{t-1} = \sum_{i=1}^{I} R_i \cdot y_{t,i}, \quad \forall t \in T \tag{19}$$

$$0 \leq y_{t,i} \leq 1, \quad \forall t \in T, i \in I \tag{20}$$

$$\sum_{i=1}^{I} y_{t,i} = 1, \quad \forall t \in T \tag{21}$$

$$\begin{bmatrix} y_{t,1} \\ y_{t,2} \\ \vdots \\ y_{t,I} \end{bmatrix} \leq \begin{bmatrix} \mathbf{H} \end{bmatrix} \begin{bmatrix} b_{t,1} \\ b_{t,2} \\ \vdots \\ b_{t,I-1} \end{bmatrix} \tag{22}$$

$$\sum_{i=1}^{I-1} b_{t,i} = 1, \quad \forall t \in T \tag{23}$$

$$\Delta soe_t = \sum_{i=1}^{I} F_i \cdot y_{t,i}, \quad \forall t \in T \tag{24}$$

$$ch_t \leq \frac{\Delta soe_t}{\Delta t \cdot \eta^{\mathrm{E}}}, \quad \forall t \in T \tag{25}$$

Equation (19) defines state of energy at the soe–Δsoe curve at the previous time period, which is used to assess the energy charging capability in hour t. Parameter R_i sets thresholds in battery's energy absorption ability (see Fig. 6), while I is the total number of thresholds (number of breakpoints of the piecewise linear approximation). $y_{t,i}$ is a continuous variable that takes values between zero and one, eq. (20), and defines which thresholds R_i are active. At most two thresholds can be (partially) active at the same time period. For instance, if $soe_t = R_2$, then $y_{t,2}$ should be equal to one, and all other $y_{t,i}$ equal to zero. In another case, if soe_t is halfway between R_2 and R_3, both $y_{t,2}$ and $y_{t,3}$ should be equal to 0.5, and all other $y_{t,i}$ equal to zero. Equation (21) therefore sets the sum of all $y_{t,i}$ to one, while eq. (22) ensures adjacency of the non-zero $y_{t,i}$ elements. Binary variable $b_{t,i}$ is used to select the piecewise line segment on which the soe_t lies. $\mathbf{H}$ is an $I \times (I-1)$ matrix with values 1 on elements (i, i) and

$(i+1, i)$, and 0 otherwise. Since variable $b_{t,i}$ is binary, eq. (23) allows only one element of $b_{t,i}$ to take value one, so only the adjacent y_t elements can be greater than zero. Equation (24) uses variable $y_{t,i}$ to assign an appropriate value to Δsoe_t based on the soe_{t-1} value. After calculating Δsoe_t in (19)-(24), charging power is limited to the maximum amount of energy that can be charged in a single time step in constraint (25).

Additional details on using SOS2, commonly used to model piecewise approximations of single variable functions, can be found in [33].

If the soe–Δsoe curve of the energy charging model is approximated using SOS2, the formulation of the bidding problem reads:

$$\text{Maximize} \quad (5)$$

subject to

$$(7) - (12), (19) - (25).$$

References

[1] DoE Global Energy Storage Database. [Online]. Available at: www.energystorageexchange.org

[2] S. Jaffe and K. Adamson, "Advanced Batteries for Utility-Scale Energy Storage," Technical Report, Navigant, 2014.

[3] H. Pandžić, Y. Wang, T. Qiu, Y. Dvorkin and D. Kirschen, "Near-Optimal Method for Siting and Sizing of Distributed Storage in a Transmission Network," *IEEE Trans. Power Syst.*, vol. 30, no. 5, pp. 2288–2300, Sept. 2015.

[4] Y. Wen, C. Guo, D. S. Kirschen and S. Dong, "Enhanced Security-Constrained OPF With Distributed Battery Energy Storage," *IEEE Trans. Power Syst.*, vol. 30, no. 1, pp. 98–108, Jan. 2015.

[5] Y. Wen, C. Guo, H. Pandžić and D. S. Kirschen, "Enhanced Security-Constrained Unit Commitment With Emerging Utility-Scale Energy Storage," *IEEE Trans. Power Syst.*, vol. 31, no. 1, pp. 652-662, Jan. 2016.

[6] F. Luo, K. Meng, Z. Y. Dong, Y. Zheng, Y. Chen and K. P. Wong, "Coordinated Operational Planning for Wind Farm With Battery Energy Storage System," *IEEE Trans. Sust. Energy*, vol. 6, no. 1, pp. 253-262, Jan. 2015.

[7] J. Tan and Y. Zhang, "Coordinated Control Strategy of a Battery Energy Storage System to Support a Wind Power Plant Providing Multi-Timescale Frequency Ancillary Services," *IEEE Trans. Sust. Energy*, vol. 8, no. 3, pp. 1140-1153, July 2017.

[8] T. Dragičević, H. Pandžić, D. Škrlec, I. Kuzle, J. M. Guerrero and D. S. Kirschen, "Capacity Optimization of Renewable Energy Sources and Battery Storage in an Autonomous Telecommunication Facility," *IEEE Trans. Sust. Energy*, vol. 5, no. 4, pp. 1367-1378, Oct. 2014.

[9] G. Liu, Y. Xu and K. Tomsovic, "Bidding Strategy for Microgrid in Day-Ahead Market Based on Hybrid Stochastic/Robust Optimization," *IEEE Trans. Smart Grid*, vol. 7, no. 1, pp. 227–237, Jan. 2016.

[10] M. González Vayá and G. Andersson, "Optimal Bidding Strategy of a Plug-In Electric Vehicle Aggregator in Day-Ahead Electricity Markets Under Uncertainty," *IEEE Trans. Power Syst.*, vol. 30, no. 5, pp. 2375–2385, Sept. 2015.

[11] H. Wu, M. Shahidehpour, A. Alabdulwahab and A. Abusorrah, "A Game Theoretic Approach to Risk-Based Optimal Bidding Strategies for Electric Vehicle Aggregators in Electricity Markets With Variable Wind Energy Resources," *IEEE Trans. Sust. Energy*, vol. 7, no. 1, pp. 374-385, Jan. 2016.

[12] S. I. Vagropoulos and A. G. Bakirtzis, "Optimal Bidding Strategy for Electric Vehicle Aggregators in Electricity Markets," *IEEE Trans. Power Syst.*, vol. 28, no. 4, pp. 4031-4041, Nov. 2013.

[13] M. R. Sarker, H. Pandžić and M. A. Ortega-Vazquez, "Optimal Operation and Services Scheduling for an Electric Vehicle Battery Swapping Station," *IEEE Trans. Power Syst.*, vol. 30, no. 2, pp. 901-910, March 2015.

[14] Y. Zheng, Z. Y. Dong, Y. Xu, K. Meng, J. H. Zhao and J. Qiu, "Electric Vehicle Battery Charging/Swap Stations in Distribution Systems: Comparison Study and Optimal Planning," *IEEE Trans. Power Syst.*, vol. 29, no. 1, pp. 221-229, Jan. 2014.

[15] M. R. Jongerden and B. R. Haverkort, "Which Battery Model to Use?," *IET Software*, vol. 3, no. 6, pp. 445-457, May 2009.

[16] M. Doyle, T. F. Fuller and J. Newman, "Modeling of Galvanostatic Charge and Discharge of the Lithium/Polymer/Insertion Cell," *J. Electrochem. Soc.*, vol. 140, no. 6, pp. 1526-1533, Jan. 1993.

[17] FORTRAN Programs for the Simulation of Electrochemical Systems. [Online]. Available at: http://www.cchem.berkeley.edu/jsngrp/fortran.html

[18] B. Homan, G. J. M. Smit, R. P. van Leeuwen, M. V. ten Kortenaar and B. V. Ten, "A Comprehensive Model for Battery State of Charge Prediction," IEEE PowerTech, Manchester, 2017.

[19] J. F. Manwell and J. G. McGowan, "Lead Acid Battery Storage Model for Hybrid Energy Systems," *Solar Energy*, vol. 50, no. 5, pp. 399-405, May 1993.

[20] D. N. Rakhmatov and S. B. K. Vrudhula, "An Analytical High-level Battery Model for Use in Energy Management of Portable Electronic Systems," IEEE/ACM International Conference on Computer Aided Design, San Jose, 2001.

[21] A. Sakti, K. G. Gallagher, N. Sepulveda, C. Uckun, C. Vergara, F. J. de Sisternes, D. W. Dees and A. Botterud, "Enhanced representations of lithium-ion batteries in power systems models and their effect on the valuation of energy arbitrage applications," *J. Power Sources*, vol. 342, pp. 279-291, Feb. 2017.

[22] Terna storage overview. [Online]. Available at: www.terna.it/engb/azienda/chisiamo/ternastorage.aspx

[23] T. B. Reddy and D. Linden, "Linden's Handbook of Batteries," 4th ed., The McGraw-Hill Companies Inc., 2011.

[24] I. Buchmann, "Batteries in a Portable World," 4th ed., Cadex Electronics Inc., 2016.

[25] S. M. Rezvanizaniani, J. Lee, Z. Liu and Y. Chen, "Review and recent advances in battery health monitoring and prognostics technologies for electric vehicle (EV) safety and mobility," *J. Power Sources*, vol. 256, pp. 110-124, June 2014.

[26] S. Piller, M. Perrin and A. Jossen, "Methods for state-of-charge determination and their applications," *J. Power Sources*, vol. 96, pp. 113-120, Jan. 2001.

[27] W. Y. Chang, "The State of Charge Estimating Methods for Battery: A Review," *ISRN Appl. Math.*, vol. 2013, Article ID 953792, 2013.

[28] K. S. Ng, C. S. Moo, Y. P. Chen and Y. C. Hsieh, "Enhanced coulomb counting method for estimating state-of-charge and state-of-health of lithium-ion batteries," *Appl. Energy*, vol. 86, pp. 1506-1511, Nov. 2008.

[29] O. Sundstrom and C. Binding, "Flexible Charging Optimization for Electric Vehicles Considering Distribution Grid Constraints," *IEEE Trans. Smart Grid*, vol. 3, no. 1, pp. 26-37, March 2012.

[30] M. R. Sarker, M. D. Murbach, D. T. Schwartz and M. A. Ortega-Vazquez, "Optimal operation of a battery energy storage system: Trade-off between grid economics and storage health," *Electric Power Systems Research*, vol. 152, pp. 342-349, Nov. 2017.

[31] European Power Exchange. [Online]. Available at: www.epexspot.com/en/

[32] Croatian Energy Regulatory Agency, "Methodology for Determining the Price for the Settlement of Balancing Energy." Zagreb, Croatia, 2016.

[33] C. Guéret, C. Prins and M. Sevaux, "Applications of optimization with Express-MP," English translation by S. Heipcke [Online]. Available at: http://www.maths.ed.ac.uk/hall/Xpress/FICO_Docs/Xpress-booka4.pdf